JACS
JOURNAL OF THE AMERICAN CHEMICAL SOCIETY
Article
pubs.acs.org/JACS

Excitonic Interfacial Proton-Coupled Electron Transfer Mechanism in the Photocatalytic Oxidation of Methanol to Formaldehyde on TiO_2(110)

Annapaola Migani*,† and Lluís Blancafort*,‡

†Catalan Institute of Nanoscience and Nanotechnology (ICN2), CSIC and The Barcelona Institute of Science and Technology, Campus UAB, Bellaterra, 08193 Barcelona, Spain

‡Institut de Química Computacional i Catàlisi and Departament de Química, Facultat de Ciències, Universitat de Girona, C/M. A. Campmany 69, 17003 Girona, Spain

Supporting Information

ABSTRACT: CH_3OH on a single-crystal rutile TiO_2(110) surface is a widely studied model system for heterogeneous photocatalysis. Using spin-polarized density functional theory with a hybrid functional (HSE06), we study the photocatalytic oxidation of CH_3OH adsorbed at a coordinately unsaturated Ti site as an excited-state process with triplet spin multiplicity. The oxidation to CH_2O is stepwise and involves a CH_3O intermediate. The first O−H dissociation step follows an excitonic interfacial proton-coupled electron transfer mechanism where the hole−electron (h−e) pair generated during the excitation is bound, and the h is transferred to the adsorbate. The O−H dissociation paths associated with other h−e pairs are unreactive, and the moderate experimental efficiency is due to the different reactivity of the h−e pairs. The excited-state CH_3O intermediate further deactivates through a seam of intersection between the ground and excited states. It can follow three different paths, regeneration of adsorbed CH_3OH or formation of the ground-state CH_3O anion or an adsorbed CH_2O radical anion. The third channel corresponds to photochemical CH_2O formation from CH_3OH, where a single photon induces one electron oxidation and transfer of two protons. These results expand the current view on the photocatalysis of CH_3OH on TiO_2(110) by highlighting the role of excitons and showing that adsorbed CH_3OH may also be an active species in the photocatalytic oxidation to CH_2O.

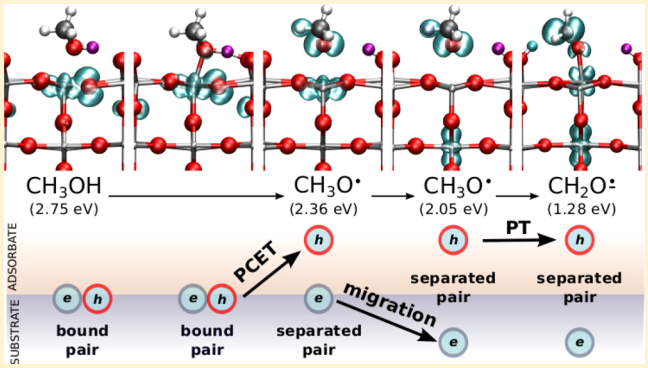

1. INTRODUCTION

TiO_2 based heterogeneous photocatalysis and photoelectrocatalysis have a very important potential role for the production of fuels and chemicals and environmental remediation.[1−4] Because of its stability, the rutile TiO_2(110) surface is an ideal substrate for model surface science studies where H_2O or CH_3OH are adsorbed under ultrahigh vacuum (UHV) conditions. A series of photochemical studies on these systems have been conducted using different techniques in combination with laser UV irradiation.[5−17] These studies under well-defined reaction conditions aim at providing insight into the elementary steps that compose the photochemical mechanism and understanding the fundamental principles of photocatalysis. This fundamental knowledge will benefit the improvement or development of technologies based on heterogeneous photocatalysis and photoelectrocatalysis.

In particular, H_2O photocatalysis on TiO_2(110)[5,6] has been studied because of its relation to photoelectrocatalytic H_2O splitting on titania.[1] CH_3OH photocatalysis on TiO_2(110)[7−17] has been investigated because of its important role in the enhancement of photoelectrocatalytic H_2 production,[18] and because of its relation with the selective photooxidation of alcohols by TiO_2 based photocatalysts.[19,20] Finally, CH_3OH photocatalysis provides an interesting contrast to H_2O photocatalysis on titania.

Scanning tunneling microscopy (STM) experiments have shown that CH_3OH adsorbed on a coordinately unsaturated Ti (Ti_{cus}) site can be photocatalytically dissociated under 400 nm light irradiation into a methoxy CH_3O group at a Ti_{cus} site and a H atom at an adjacent bridging O (O_{br}), i.e., $O_{br}H$ group[7] (structures **1A** and **1B**, Figure 1). The light wavelength is consistent with the bulk rutile TiO_2 optical band gap of 3.03 eV,[21,22] indicating that the photodissociation is a photocatalytic process.

Photodissociation experiments conducted for H_2O adsorbed at a Ti_{cus} site of rutile TiO_2(110)[5] support the participation of photogenerated holes in the photocatalytic O−H bond

Received: October 24, 2016
Published: November 17, 2016

DOI: 10.1021/jacs.6b11067
J. Am. Chem. Soc. 2016, 138, 16165−16173

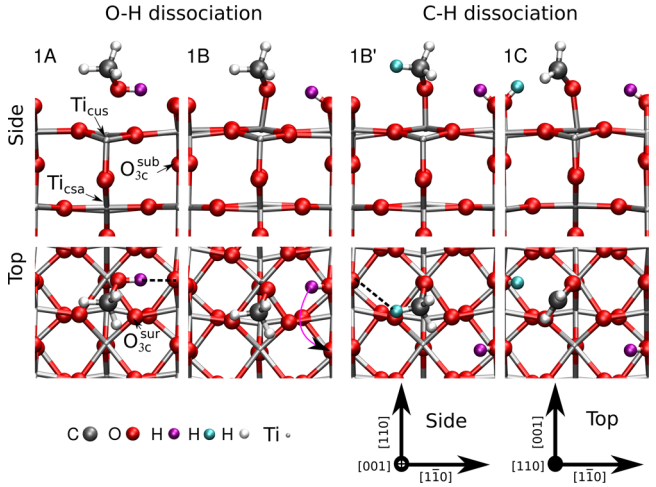

Figure 1. Schematics for the double, stepwise dissociation of 1/2 ML CH_3OH adsorbed at a Ti_{cus} site of a $TiO_2(110)$ 2 × 1 supercell, duplicated along the [001] direction (side and top views). **1A** represents adsorbed CH_3OH, **1B** and **1B′** adsorbed CH_3O and an $O_{br}H$ group, and **1C** adsorbed CH_2O and two $O_{br}H$ groups. The H atoms dissociated in the first and second steps are marked in magenta and cyan, respectively. The dashed lines in **1A** and **1B′** (top view) connect the substrate's O_{br} and adsorbate's H atoms involved in the interfacial H transfers. The arrow in **1B** (top view) indicates the displacement of the H dissociated in the first step from the O_{br} adjacent to the occupied Ti_{cus} site to the O_{br} adjacent to the empty Ti_{cus} site. Subsurface 3-fold coordinated O (O_{3c}^{sub}), surface 3-fold coordinated O (O_{3c}^{sur}), Ti_{cus}, and coordinately saturated Ti (Ti_{csa}) are labeled.

dissociation, which suggests that the same mechanism may apply for adsorbed CH_3OH. Moreover, proton-coupled electron transfer (PCET) has been shown to be of general importance in heterogeneous photocatalysis.[23−25] For example, ultrafast two-photon photoemission experiments on methanol covered rutile $TiO_2(110)$ surfaces have shown that PCET is the mechanism that stabilizes the negative charge induced on the methanol overlayer by electron excitation to the so-called "wet electron" state.[26−28] In this context, density functional theory (DFT) calculations on the dissociation of water, organic alcohols, formaldehyde, and formic acid on anatase $TiO_2(101)$ suggest that the photocatalytic O−H bond dissociation may also follow an interfacial PCET mechanism,[29−31] mediated by so-called "free hole" states,[30] and "trapped hole" states.[31]

While most theoretical studies have focused on the nature of the *h* to understand the O−H dissociation,[30,32−34] the role of exciton states in this essential step of the photocatalytic mechanism has not been considered. Usually the photocatalytic oxidation is described as an interfacial electron transfer between the catalyst and the reactant involving valence band (VB) holes that are "independent" of the conduction band (CB) electrons.[2] In contrast, in the excitonic state the hole (*h*) and the electron (*e*) are bound. In this work we address the role of exciton states with a perspective similar to that of molecular photochemistry and we consider the specific reactivity of different excitonic configurations. Under this view, the trapping site of the *h* depends on the configuration of the excitonic state during the redox process, prior to the charge carrier separation, and this plays a key role in the efficiency.

Photocatalytic O−H bond dissociation is also relevant in the context of methanol oxidation to formaldehyde CH_2O.[8,10,13−17] This reaction involves the cleavage of the O−H bond (structures **1A** and **1B**) and one C−H bond (structures **1B′** and **1C**), resulting in the CH_2O species adsorbed at a Ti_{cus} site and two $O_{br}H$ groups. In the most widely accepted stepwise mechanism the O−H bond dissociation precedes the C−H bond dissociation. This mechanism goes through the ground-state adsorbed CH_3O intermediate, and both steps are photoinitiated.[8] CH_2O is also obtained from across band gap photoexcitation of a pure layer of adsorbed CH_3O species, which is formed by coadsorbing CH_3OH with O atoms.[11,35] These experiments provide evidence for the CH_3O adsorbate being the active species for *h* mediated oxidation of CH_3O on $TiO_2(110)$ forming CH_2O. This mechanistic picture has been confirmed theoretically in two different dynamics studies, showing that the *h* can become localized only on adsorbed CH_3O species,[34] and that the excited CH_3O radical undegoes C−H bond dissociation to form formaldehyde.[36]

In contrast, in recent STM experiments combined with laser irradiation at 355 nm only direct methanol dehydrogenation to adsorbed formaldehyde was imaged, and no evidence for the adsorbed CH_3O intermediate was obtained.[16] These results have been interpreted as simultaneous rather than stepwise bond cleavage of the O−H and C−H bonds, and suggest that adsorbed CH_3OH itself may be an active species in the photocatalytic oxidation to CH_2O. X-ray photoelectron spectroscopy experiments also provide direct evidence that the photocatalytic dissociation of methanol contributes to the photocatalytic oxidation of methanol on the $TiO_2(110)$ surface.[13] In these experiments the mechanism of formaldehyde formation from methanol is relevant for the efficiency of formation of methyl formate from the formaldehyde intermediate.[13]

These two issues, the excitonic PCET mechanism of the O−H bond dissociation and its relationship with the formation of CH_2O, are the main focus of this paper. Our computational model is 1/2 ML CH_3OH adsorbed at a Ti_{cus} site of a $TiO_2(110)$ slab treated with spin-polarized DFT with the HSE06[37] variant of the hybrid exchange-correlation functional HSE.[38] The hole−electron (*h*−*e*) pairs describing the excitonic state are represented as a triplet spin multiplicity state, i.e., T_1 state, which allows to consider the synergistic catalytic role of holes and electrons.

Our study addresses several open questions. The first significant problem for the *h* mediated mechanism is represented by the unfavorable interfacial level alignment of the CH_3OH highest occupied levels relative to the $TiO_2(110)$ valence band maximum (VBM). Based on ultraviolet photoemission spectroscopy (UPS)[39] and many-body quasiparticle (QP) GW calculations[40−42] the CH_3OH highest occupied levels are ∼1.3 eV below the $TiO_2(110)$'s VBM. Thus, the *h* transfer from the $TiO_2(110)$ VBM to the CH_3OH highest occupied molecular orbital (HOMO) is thermodynamically forbidden, as shown in Figure 2a. For methanol on anatase $TiO_2(101)$ it has been shown that concerted PCET results in almost complete oxidation of the methanol molecule.[30] However, this case is more favorable than the case of methanol on rutile $TiO_2(110)$. This is because of the more favorable interfacial level alignment in anatase $TiO_2(101)$ compared to rutile $TiO_2(110)$ substrates, as indicated by the comparison of the interfacial level alignment of water on rutile $TiO_2(110)$ and anatase $TiO_2(101)$.[43] Still, we will show below that the mechanism found for anatase $TiO_2(101)$ applies also for methanol on rutile $TiO_2(110)$. The proton transfer provides

DOI: 10.1021/jacs.6b11067
J. Am. Chem. Soc. 2016, 138, 16165−16173

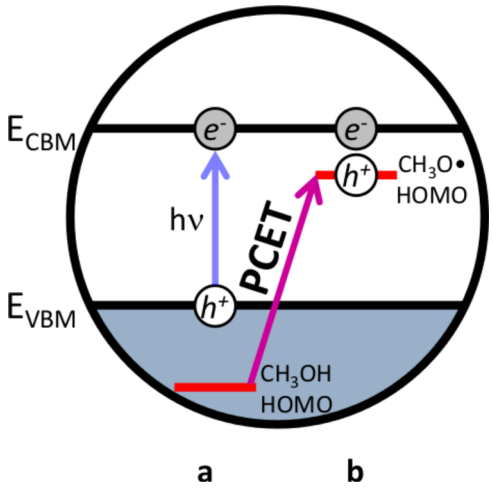

Figure 2. Schematic interfacial level alignment of CH_3OH HOMO with respect to TiO_2(110) VBM and CBM (a) before and (b) after O−H bond dissociation.

the chemical energy needed to raise the HOMO above the VBM (Figure 2b) and localize the *h* on methanol.

Moreover, it is not clear how the participation of photogenerated holes in the photocatalytic O−H bond dissociation would result in the formation of an anionic methoxy species that is not oxidized (structures **1B** and **1B′**). In this respect, we will highlight the importance of distinguishing two electronic configurations for the adsorbed CH_3O species, a closed-shell ground-state anion and an excited-state radical.

Another open question is whether CH_3OH is also a reactive species for *h* mediated oxidation to CH_2O. In other words, it remains unclear whether the photocatalytic conversion of adsorbed CH_3OH to adsorbed CH_2O goes necessarily through the ground-state adsorbed CH_3O species (structures **1B** and **1B′**),[8] which would correspond to a two-photon process, or whether it can occur as a one-photon process that does not involve the ground-state adsorbed CH_3O intermediate.[16] We will present a global mechanistic picture showing that our excitonic PCET mechanism is connected to the one- and two-photon pathways of CH_2O formation, where the two adsorbed CH_3O electronic configurations have a key role.

2. COMPUTATIONAL DETAILS

All HSE06 DFT calculations are performed using VASP within the projector augmented wave (PAW) scheme.[44] HSE06[37] provides the best absolute alignment of the conduction band minimum (CBM) and VBM for the H_2O on TiO_2(110) interface[45] and the clean TiO_2(110) surface.[41] Moreover, it provides accurate electronic band gaps for rutile and anatase TiO_2[41,43] and cathecol on TiO_2(110) interfaces.[46−48] To model the exciton state it is necessary to compute an excited state where the *e* is promoted to the CB, leaving a *h* in the VB. The excited state is modeled as the lowest triplet state T_1 because the alternative of optimizing the lowest singlet S_1 excited-state paths, for example using the Bethe Salpeter method,[48−50] is not feasible for our system. We expect the T_1 and S_1 states will differ at most by a few tenths of eV and that the mechanistic picture will not change. In order to achieve localization of the *h* and *e* at different O and Ti sites, respectively, we have modified the position of these atoms with respect to those of the ground-state adsorbed intact and dissociated methanol minima.

The geometries are fully relaxed with all forces $\lesssim$0.02 eV/Å. We employ a plane-wave energy cutoff of 445 eV, an electronic temperature $k_BT \approx 0.2$ eV with all energies extrapolated to $T \to 0$ K, and a PAW pseudopotential for Ti which includes the $3s^2$ and $3p^6$ semicore levels. All unit cells contain a TiO_2(110) slab made of five triatomic thick layers, employ the experimental lattice parameters for bulk rutile TiO_2 (a = 4.5941 Å, c = 2.958 Å),[51] and include at least 10 Å of vacuum between repeated images. To model 1/2 ML coverage, we repeat the TiO_2(110) 1 × 1 unit cell along the [001] direction. Since the slabs considered exhibit nonzero dipole moments along the [110] direction, dipole corrections have been applied to the potential, total energies and forces.

We use the climbing-image nudged elastic band (CI-NEB)[52] method to compute the O−H bond and C−H bond dissociation reaction coordinates and barriers with four intermediate images. The starting geometries of the images are obtained interpolating the geometries of reactant and product minima with the centers of mass aligned with the "intpol" routine of the AFLOW program.[53] All calculations are performed employing the Γ-point only. All T_1 calculations and the NEB calculation for the S_0 C−H bond dissociation are performed spin polarized, while the NEB calculation for the S_0 O−H bond dissociation is performed spin unpolarized.

The T_1 excitation energy of the interface at the reactant geometry is ∼3.18 eV, in agreement with the optical band gap of rutile TiO_2.[21,22,41,43] This T_1 excitation energy is used as the energy reference to assess the feasibility of the different O−H dissociation paths.

The adsorption energy E_{ads} is given by

$$E_{ads} \approx E[\text{methanol} + TiO_2(110)] - E[TiO_2(110)] - E[\text{methanol}] \quad (1)$$

where E[methanol + TiO_2(110)], E[TiO_2(110)], and E[methanol] are the total energies of the covered and clean surfaces and gas phase methanol molecule, respectively. The computed adsorption energy for 1/2 ML methanol adsorbed at a Ti_{cus} site is ∼ −0.95 eV. This value is in very good agreement with previously reported values.[54,55]

On a real surface, the O−H and C−H dissociation steps involve the two O_{br} atoms marked with dashed lines in the top views of structures **1A** and **1B′** (Figure 1), respectively.[16,17] However, in our TiO_2(110) 2 × 1 supercell these two atoms are equivalent and correspond to the same site. As a result, transfer of both H atoms to this site is not possible. This problem would be avoided by using a 2 × 2 supercell, duplicated in the [1$\bar{1}$0] direction. However, this is not affordable computationally. Instead, after the O−H dissociation step we move the dissociated H atom to the O_{br} atom adjacent to the empty Ti_{cus} site, to allow for the second interfacial H transfer. This leads to structure **1B′** in Figure 1. Accordingly, the C−H bond dissociations in the ground and excited states are studied using the **1B′** model. This is a good approximation, because the energy of the ground- and excited-state minima for adsorbed CH_3O is almost independent of the position of the dissociated H atom (Figure S1 in Supporting Information and structures **1g** and **1g′** below).

3. RESULTS AND DISCUSSION

3.1. Excited-State O−H Bond Dissociation Mechanism. Electronic excitation near the band gap energy of CH_3OH adsorbed at a Ti_{cus} site of TiO_2(110) results in the formation of bulk delocalized excitons. Nuclear relaxation after excitation results in different minima with different electronic configurations, corresponding to different locations of the *h* and *e*. To identify the electronic configuration responsible for the photocatalytic activity, we computed various O−H bond dissociation paths associated with different electronic configurations. These correspond to *h* localization at four different O sites and *e* localization at two different Ti sites. The first two O sites are the two bridging O atoms (O_{br}) with and without H bond with the CH_3OH adsorbate, which are adjacent to the occupied and empty Ti_{cus} sites, respectively. The other two O sites are a subsurface 3-fold coordinated O (O_{3c}^{sub}), and a surface 3-fold coordinated O (O_{3c}^{sur}) (Figure 1). To understand the effect of the *h* and *e* separation distance on the O−H

DOI: 10.1021/jacs.6b11067
J. Am. Chem. Soc. 2016, 138, 16165−16173

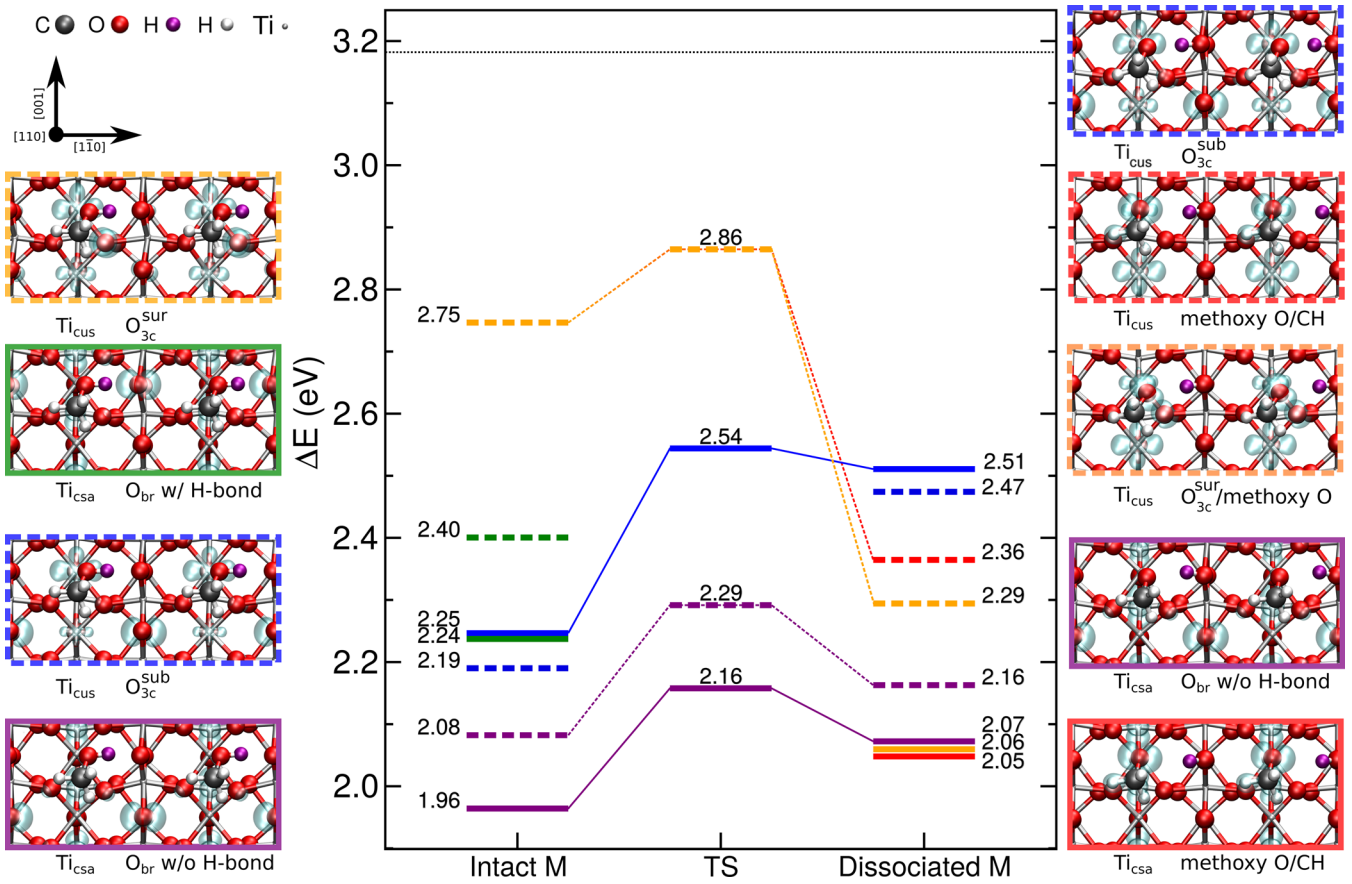

Figure 3. Energy profiles of O−H dissociation paths for different excited-state T_1 configurations of 1/2 ML CH_3OH adsorbed at a Ti_{cus} site. Energies in eV relative to the S_0 energy of the intact CH_3OH minimum. The color code indicates *h* localization. Purple: *h* at bridging O (O_{br}) atom without H bond with the CH_3OH adsorbate; blue: *h* at subsurface 3-fold coordinated O (O^{sub}_{3c}) atom; green: *h* at O_{br} with H-bond with the CH_3OH adsorbate; orange: *h* at surface 3-fold coordinated O (O^{sur}_{3c}) for intact CH_3OH, and *h* shared between the O^{sur}_{3c} atom and the terminal methoxy O atom for dissociated CH_3OH; red: *h* shared between the terminal methoxy O atom and the C−H bond (methoxy O/CH) for dissociated CH_3OH. The change from orange to red in one of the paths indicates a change in *h* position. Solid and dashed lines indicate *e* localization at Ti_{csa} or Ti_{cus} sites, respectively. The orange and red paths follow the exothermic PCET mechanism, while the other paths follow an endothermic PT mechanism. Spin densities are shown for selected *h*−*e* pairs indicating the *h* and *e* localization site. The 1 × 2 unit cell is duplicated along the [1$\bar{1}$0] direction in the T_1 spin densities' representation.

dissociation energetics, we considered *e* localization at two different Ti sites, a coordinately unsaturated one, Ti_{cus}, and a saturated one in the second layer, Ti_{csa} (Figure 1).

For the interface with adsorbed intact CH_3OH, we located the relaxed minima for seven possible electronic configurations and computed the photodissociation coordinate for four of them. The energies of reactants, transition states and products are presented together with the most relevant spin densities in Figure 3. Different colors correspond to different *h* locations, and solid and dashed frames and lines correspond to *e* localization at the Ti_{csa} and Ti_{cus} sites, respectively. The preferred T_1 configurations by ∼0.1−0.2 eV occur for the charge carriers' largest separation. Thus, the most stable configuration with the *h* at non H-bonded or H-bonded O_{br} atom has the *e* at the Ti_{csa} site (solid purple and green, respectively), and the most stable configuration with the *h* at the O^{sub}_{3c} atom has the *e* at the Ti_{cus} site (dashed blue). These data indicate a weak interaction between the *h* and the *e* for the electronic configurations with the *h* at the O_{br} and O^{sub}_{3c} sites and the propensity for the *h* at these sites to separate from the *e*.

The O^{sur}_{3c} site is the most relevant one for the oxidation of adsorbed CH_3OH because the *h* is close to the CH_3OH adsorbate, which is a necessary condition for *h* transfer. *h* localization at this site could only be achieved localizing the *e* at the Ti_{cus} site (dashed orange). This indicates a strong interaction between the *h* and *e* and shows that the transfer of the *h* to the photocatalyst surface goes through a bound exciton.

The paths are obtained connecting reactant and product minima with the same excitonic configuration. With this approach we avoid discontinuities along the paths due to sudden changes of electronic configuration. For the product minimum with Ti_{cus}/methoxy configuration (dashed red Dissociated M in Figure 3) there is no counterpart with the same configuration on the reactant side. In this case we start the path from the Ti_{cus}/O^{sur}_{3c} reactant configuration (dashed orange Intact M in Figure 3) because for this minimum we already observe the incipient interaction between the methanol O and the O^{sur}_{3c} site which is preparatory for the *h* transfer to the methoxy group.

All the relaxed T_1 electronic configurations for the interface with adsorbed intact CH_3OH as well as the dissociation paths are below the vertical excited-state energy of ∼3.18 eV, represented as a horizontal line in Figure 3. This implies that all excited-state paths are accessible energetically.

DOI: 10.1021/jacs.6b11067
J. Am. Chem. Soc. 2016, 138, 16165−16173

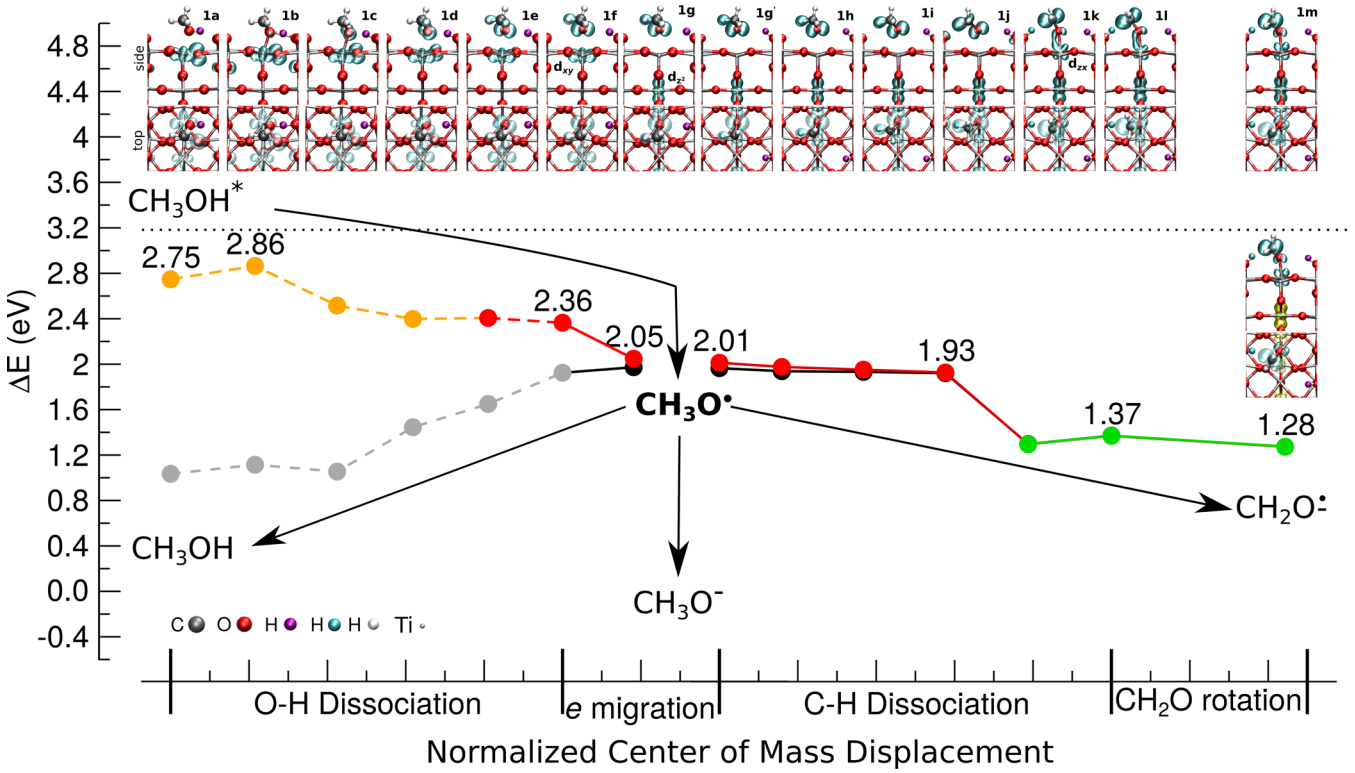

Figure 4. T_1 and S_0 energies, structures and spin densities for excited CH_3OH (CH_3OH^*) to CH_2O radical anion photocatalytic oxidation on the T_1 state for 1/2 ML CH_3OH adsorbed at Ti_{cus}. This process involves three main steps: (1) O−H bond dissociation via PCET mechanism (structures **1a**−**1f**); (2) Ti_{cus} to Ti_{csa} *e* migration involving the $3d_{xy}$ and $3d_{z}^2$ orbitals (**1f** and **1g**, respectively); (3) C−H σ bond acidic dissociation (**1g′**−**1m**). Structures **1g** and **1g′** correspond to T_1 excited-state adsorbed methoxy radical, and **1m** to the adsorbed CH_2O radical anion. The spin density of the singlet CH_2O radical anion is shown for comparison. The competing deactivation paths of the CH_3O radical leading to CH_3OH regeneration and formation of the ground-state CH_3O anion are included. Energies relative to the S_0 energy for the intact CH_3OH minimum; in the final part (**1g**−**1m**), the S_0 and T_1 energies are degenerate. A change in color across connected points indicates a change in the *h* position. Dashed lines indicate a bound T_1 *h*−*e* pair (orange) or S_0 closed-shell configuration (gray); solid lines indicate separated T_1 (red, green) or S_0 (black) *h*−*e* pairs.

The calculated paths show two alternative proton transfer (PT) mechanisms, one where the *h* participates in the photodissociation and one where it does not. Remarkably, only the path that involves the *h* in the dissociation is exothermic by ∼0.4−0.5 eV (dashed orange and red paths in Figure 3), and it is only slightly activated (∼0.11 eV). This path can lead to two different minima, one with the hole shared between the adsorbate and the substrate (dashed orange Dissociated M), which has the same electronic configuration as the reactant minimum, and another one with the hole fully localized on the adsorbate (dashed red Dissociated M). In this latter case, the *h* is transferred from the O_{3c}^{sur} of the substrate to the adsorbate, inducing the oxidation of the adsorbate. At the same time a proton is transferred from the CH_3OH adsorbate to the O_{br} of the TiO_2(110) substrate. This results in a decrease in the activation barrier and stabilization of the product minimum relative to the reactant minimum. This mechanism corresponds to a concerted PCET process,[56] which is also well-known from molecular photochemistry.[57−61] The ET step can be regarded as the opposite of the *h* transfer step, i.e., from the adsorbate to the substrate. The *h*-shared configuration can be considered a precursor for *h* localization at the adsorbate. All the other T_1 photodissociation paths (blue and purple paths in Figure 3) have a larger activation barrier (∼0.2−0.3 eV) and are endothermic (∼0.1−0.3 eV). These paths are not relevant for the CH_3OH oxidation as the *h* remains on the TiO_2 substrate. This mechanism can be described as a PT process. While the PT endothermic paths are reversible, the exothermic PCET path is irreversible and is the one ultimately responsible for the photooxidation of adsorbed methanol.

A stabilization by ∼0.2−0.3 eV of the shared- and localized-*h* configurations is computed upon *e* migration from the bare Ti_{cus} site to the Ti_{csa} site (solid orange and red dissociated M in Figure 3, respectively), which results into separated *h*−*e* pairs. These structures correspond to the lowest-energy minima on the product side of the diagram. The charge-separated structure with the *h* fully localized at the adsorbate, corresponds to an excited-state adsorbed methoxy radical minimum. Overall, Figure 3 shows that this species is formed via the PCET coordinate followed by *h*−*e* pair separation. In contrast, the endothermic O−H dissociation paths are likely to revert under UHV conditions. They may result in the regeneration of the reactant minimum with the *h* localized on the O_{br} site adjacent to the empty Ti_{cus} site (solid purple Intact M in Figure 3), which has the largest relaxation energy (∼1.22 eV with respect to the vertical excitation energy). This minimum is catalytically inert under UHV and will undergo charge carrier recombination to return to ground-state adsorbed CH_3OH.

The configurations which are photocatalytically inactive here may become relevant under different conditions. For higher coverage under UHV, adsorption of a second methanol layer coordinated to the O_{br} sites will block the O−H dissociation of adsorbed CH_3OH, as suggested by a combined experimental and theoretical study.[62] Under these conditions, the second methanol layer may be photocatalytically oxidized by the excitons with the *h* located at the O_{br} sites (framed green and

DOI: 10.1021/jacs.6b11067
J. Am. Chem. Soc. 2016, 138, 16165−16173

purple in Figure 3).[31,32] These configurations may be also important in the photooxidation of organic pollutants in solvated media[2,3] because they have a reactive O_{br} radical species at the surface.

Figure 4 shows the details of the exothermic PCET O−H photodissociation path in the context of CH_2O formation. It starts from the minimum with the *h* located at the O_{3c}^{sur} atom (**1a** in Figure 4 and dashed orange Intact M in Figure 3). Due to the unfavorable level alignment, the *h* transfer from the $TiO_2(110)$ substrate to the CH_3OH adsorbate needs the chemical energy originating from the proton transfer. The *h* transfer is gradual and is mediated by a three-electron two-atom hemibond between the O_{3c}^{sur} 2p orbital and the methoxy O 2p orbital.[63] In structures **1a**−**1c** the *h* density dominantly resides at O_{3c}^{sur}. In structure **1d** the *h* density is mostly at the methoxy O, the CH_3O group is tilted toward the O_{3c}^{sur} atom and the O−O distance is ∼2.45 Å.

Once the proton transfer is completed, the methoxy group is lifted to a more upright position and the hemibond breaks. In structures **1e** and **1f** the *h* is fully on the adsorbate and is delocalized between the methoxy O 2p and the C−H σ orbitals. The PT and *h* localization cause a decrease of the CH_3O's charge by ∼1.0 electron relative to the ground-state adsorbed CH_3OH species, weakening the interfacial dative bond. As a result, the adsorbate O atom distance to the Ti_{cus} site, O−Ti_{cus}, increases from ∼2.03 Å to ∼2.27 Å from structure **1c** to **1f**. Therefore, a stretched Ti_{cus} bond is a fingerprint for *h* localization onto the adsorbate. In contrast, along the endothermic O−H dissociation paths (blue and purple paths in Figure 3), the O−Ti_{cus} distance progressively contracts from ∼2.1−2.2 to ∼1.8−1.9 Å, similar to what happens in the ground-state (Figure S2a). We also find a smaller decrease of the CH_3O's charge by ∼0.4 electron relative to the ground-state adsorbed CH_3OH species compared to that of the PCET coordinate.

The evolution of the spin densities and structures along the PCET path also shows that the *h*-shared configuration (**1d**) is a precursor for the *h*-localized configuration (**1f**). The interconversion between the two configurations is almost barrierless, as confirmed by computing the energy profile along an interpolated coordinate between the corresponding minima (Figure S3).

As discussed, there is a strong interaction between the *h* at O_{3c}^{sur} and *e* at the Ti_{cus} underneath the adsorbate in **1a**. Figure 4 (top view of spin densities and structures) shows the *e* density is shifted from the Ti_{cus} site underneath the CH_3OH adsorbate (**1a**−**1b**) to the neighboring, bare Ti_{cus} site (**1c**−**1d**) as the proton is transferred from the adsorbate to the substrate. At the dissociated *h*-shared and *h*-localized configurations the spatial separation between the *h* and *e* is larger, and the interaction between them is weaker. This indicates the *e* has the tendency to separate from the *h* once the *h* has been transferred to the adsorbate. Overall, these data establish the key role of the *h* in the photodissociation of CH_3OH on the $TiO_2(110)$ surface and the importance of the synergy between the *h* and *e* in the early stage of this process. Once the O−H dissociation is completed the *h*−*e* pair separates. Initially a moderate separation is manifested in a polarization of the surface Ti atoms' 3d orbital toward the empty surface Ti_{cus} site. Afterward, a clear separation is accomplished by *e* migration to a Ti_{csa} site underneath the surface, which effectively corresponds to an electronic state change due to the occupation of a different Ti 3d orbital, shown by a change of the energy profile from dashed to solid. This results in the T_1 excited-state adsorbed methoxy radical intermediate **1g**.

From a global perspective, **1g** is the hub between three pathways leading to different primary products, namely adsorbed methanol, adsorbed methoxy anion and adsorbed formaldehyde radical anion (Figure 4). The competition between these paths is discussed in the next section.

3.2. Excited-State C−H Bond Dissociation Mechanism.

Figure 4 shows that C−H dissociation converts the adsorbed methoxy radical **1g′** into an adsorbed formaldehyde radical anion **1m**. In **1g′**, the H has been moved to the O_{br} site adjacent to the empty Ti_{cus} site (see Computational Details). Top view of structures **1g′**−**1l** shows that the C−H dissociation coordinate involves a rotation of the CH_3O adsorbate around the [110] direction that brings the methyl H to an optimal position for interfacial H transfer to the O_{br} atom adjacent to the occupied Ti_{cus} site (∼1.55 Å interfacial distance). The reaction coordinate is exothermic (∼0.64 eV) and barrierless. This is consistent with the observation that the adsorbed methoxy radical electronic configuration is converted into the adsorbed formaldehyde radical anion electronic configuration via PT. Thus, this reaction corresponds to an acidic C−H dissociation.[36]

The PT leaves a negative charge on the formaldehyde adsorbate, which is stabilized by delocalization onto the substrate via the interaction of the CH_2O π and π^* levels with the Ti_{cus} d_{zx} level, with the *h* located in the nonbonding π orbital (structures **1k** and **1l**). As a result of the formation of the interfacial π bond, the O−Ti_{cus} distance between the CH_2O adsorbate and the Ti_{cus} site underneath decreases from ∼2.17 to ∼1.89 Å from **1j** to **1k** (Figure S2b). The rather abrupt energy change (∼0.6 eV) between **1j** and **1k** is related to the reordering of electronic levels, which accompanies the C−H bond breaking and results in the interaction of the π and π^* and d_{zx} levels. This indicates that the interfacial acidic dissociation of the C−H bond from the adsorbate to the substrate is coupled to partial electron transfer in the same direction, i.e., from the adsorbate to the substrate. In other words, this process can also be classified as a concerted interfacial PCET mechanism, though a complete *e* transfer is not achieved.

The adsorbed formaldehyde radical anion **1l** formed after sequential O−H and C−H bond dissociations further relaxes into a more stable adsorbed formaldehyde radical anion **1m** located at ∼1.28 eV. In this relaxation the CH_2O group rotates around the [110] direction backward to a position where the CH_2O molecular plane is essentially aligned along a surface O_{3c}−Ti_{cus} bond, so as to maximize the interaction between the formaldehyde H and the surface O_{3c} atom. This specific adsorption configuration of CH_2O at a Ti_{cus} site on $TiO_2(110)$ with $O_{br}H$ groups is evidenced in the STM experiments[16,17,64] used to follow the photodissociation of adsorbed CH_3OH on $TiO_2(110)$.

The acidic C−H dissociation was also shown to take place in an almost barrierless way when an adsorbed methoxy radical is photochemically generated on the S_1 excited state upon light irradiation of a $TiO_2(110)$ interface with CH_3O adsorbed at a Ti_{cus} site.[36] This species is experimentally formed from thermal dissociation of adsorbed CH_3OH induced by coadsorbtion of O atoms.[11,35,36] Here, we show that the adsorbed methoxy radical (**1g**, **1g′**) may be also generated following excitation of a $TiO_2(110)$ interface with intact CH_3OH adsorbed at a Ti_{cus} site via a PCET process. Therefore, a single photon may be

DOI: 10.1021/jacs.6b11067
J. Am. Chem. Soc. 2016, 138, 16165−16173

sufficient to form adsorbed formaldehyde radical anion **1m** from photoexcited adsorbed CH_3OH in a stepwise mechanism on the T_1 excited state, without going through the S_0 adsorbed CH_3O intermediate, via an only slightly activated (~0.1 eV) path. This result shows that adsorbed CH_3OH is directly connected to the adsorbed formaldehyde radical anion, and therefore is also, besides adsorbed CH_3O, an active species in the photooxidation to formaldehyde. The interaction of the excited-state adsorbed methanol with the *h* is possible thanks to the chemical energy coming from the proton transfer (see Figure 2).

The excited-state adsorbed CH_3OH to adsorbed formaldehyde radical anion transformation is exothermic (1.47 eV), while the corresponding ground-state reaction is endothermic (1.27 eV, Figure S1). Moreover, the S_0 C−H dissociation coordinate is characterized by an electronic configuration change from closed shell to open shell together with a small increase of the interfacial O−Ti_{cus} distance (Figure S2b). The singlet open-shell minimum for the adsorbed formaldehyde radical anion is degenerate with the T_1 state structure **1m**. This indicates that the transition state for the S_0 C−H dissociation coordinate is associated with an avoided crossing between the closed-shell configuration of the adsorbed methoxy anion and the open-shell configuration of the adsorbed formaldehyde radical anion. Our estimated energy barrier is 1.85 eV, which compares well with the previous estimate of 1.6 eV.[8] However, an accurate determination of the barrier height would require the use of multireference methods to account for the multiconfigurational character of the S_0 C−H dissociation coordinate.

3.3. Competing Pathways and Efficiency Considerations. The nature of the species responsible for the photocatalytic oxidation mediated by O−H dissociation on TiO_2 surfaces has been extensively discussed (see for instance refs 65−67). Previous theoretical studies have proposed different mechanisms for H transfer to the surface from water and organic molecules adsorbed at a Ti_{cus} site[30,33] or from water electrostatically coordinated to the surface,[31,32] or for H transfer to the solvent from water adsorbed at a Ti_{cus} site.[25] In the specific case of interfacial H transfer to the substrate, it has been discussed whether the oxidizing species corresponds to so-called "free hole" states where the *h* is delocalized over the substrate, or "trapped hole" states with the *h* localized on the surface, which occurs preferentially at an O_{br} site. The first possibility has been proposed for adsorbed molecules,[30,33] and the second one for electrostatically coordinated molecules.[31,32] The free hole mechanism has a lower energy barrier than the one involving trapped states,[33] but it is problematic from the point of view of kinetics because O−H dissociation has to take place before the *h* gets trapped. Our results solve this apparent controversy by showing that the species responsible for the oxidation is an exciton where the *h* is localized at the surface O_{3c} site thanks to *e* localization at the Ti_{cus} site. Thus, there is no competition between *h* trapping and O−H dissociation, but rather a sequential process consisting of localization of the photogenerated exciton and subsequent O−H dissociation. In addition, by considering the exciton the barrier is substantially lowered (by ~0.24 eV) with respect to the one calculated for the free hole state.[30]

From this perspective, the limiting factor for the photocatalytic efficiency of the first step, which is probably responsible for the low experimental yields,[7,10,15] is the localization of the photogenerated exciton to give this particular species and not the remaining, unreactive excitons. In contrast, charge carrier recombination of this exciton before O−H dissociation does not appear to be so critical in spite of the short distance between the *h* and *e*, since the probability of nonradiative recombination is low given the high energy gap between the exciton state and the neutral ground state. Charge carrier recombination via luminescence should also have a longer time scale than the O−H dissociation, which has a barrier of only ~0.11 eV. The relatively high energy of the reactive excitonic configuration for intact M may also be related to the higher yields obtained with shorter excitation wavelength.[10,15]

The formation of adsorbed formaldehyde radical anion **1m** from the **1g′** intermediate competes with formation of adsorbed methanol and adsorbed methoxy anion (Figure 4). A quantitative assessment of the product yields would require dynamics calculations which are beyond the scope of our work, but we have identified the main factor that affects the efficiency of formaldehyde formation by considering the potential energy surface topology along the reaction coordinate. In this respect, Figure 4 shows that the energy separation between the T_1 and S_0 states decreases along the PCET coordinate until they become almost degenerate at the excited-state adsorbed methoxy radical minimum (**1g**, **1g′**). Consistent with this, at **1f** the separation between the CH_3O highest occupied levels and the CBM, estimated with a 4 × 4 × 1 *k*-point mesh, is only ~0.7 eV (Figure 2b). As discussed, the adsorbate O atom distance to the Ti_{cus} site increases along the PCET coordinate (Figure S2a). The stretching of the O−Ti_{cus} distance destabilizes the S_0 state with closed-shell electronic configuration (solid gray) and stabilizes the open-shell singlet and triplet configurations. Therefore, it induces a change of the ground-state electronic configuration from closed to open shell, similar to the one described above for the ground-state C−H dissociation coordinate, and it contributes to reach the degeneracy with T_1.

State degeneracies are photochemically relevant as they mediate the radiationless transition between states and drive the formation of primary products.[68,69] The quasi-degeneracy is preserved along the C−H dissociation coordinate, where both the ground and excited states have an open-shell electronic configuration, with the unpaired electrons residing at the adsorbate and the substrate (see the triplet spin densities for **1g′**−**1m** in Figure 4). The quasi-degeneracy spans an extended section of the potential energy surface and is reminiscent of surface crossing hyperlines, i.e., seams, extensively documented in molecules.[58,70−74] A seam is composed of different segments lying along a reaction coordinate. Each segment is associated with a different primary photoproduct, and the outcome of the reaction depends on which part of seam is accessed for the deactivation.[58,70−74] Here, there is a difference between the products formed from the initial and final parts of the seam.

The initial part of the seam near the excited-state adsorbed methoxy radical is associated with the formation of S_0 adsorbed methoxy anion and adsorbed methanol, with a detrimental effect on the efficiency of formation of the adsorbed formaldehyde radical anion. This is similar to the crossing between T_1 and S_0 described for the related methanol oxidation reaction to formaldehyde on silica and titania supported vanadate sites, which also involves a methoxy-like species.[75] In that case it was demonstrated that the nonadiabatic transition plays a role in the catalytic mechanism, similar to what we propose here. In our case, the relaxation path to adsorbed

DOI: 10.1021/jacs.6b11067
J. Am. Chem. Soc. 2016, 138, 16165−16173

methanol corresponds to charge carrier recombination accompanied by back PT. This path corresponds to the dashed gray energy profile in Figure 4, which is the ground-state energy along the T_1 reaction path and provides a good approximation to the minimum energy path connecting the methoxy radical and methanol species. The relaxation path to the adsorbed methoxy anion also corresponds to charge carrier recombination. Thus, charge carrier recombination explains the formation of the not-oxidized species corresponding to adsorbed methoxy anion and adsorbed methanol after photocatalytic oxidation of adsorbed CH_3OH to the adsorbed methoxy radical (**1g**, **1g′**) followed by decay to S_0. The adsorbed methoxy anion may revert to the starting methanol species on the ground-state, thus reducing the efficiency of the first dissociation. This is consistent with the low probability of photodissociation of adsorbed CH_3OH into adsorbed CH_3O and $O_{br}H$ reported experimentally.[7]

The final part of the seam is associated with the formation of adsorbed formaldehyde radical anion **1m**. This species is a stable ground-state minimum because the last structure of the seam coincides with the degenerate minima of the ground and excited states. In contrast to the other decay paths, at this structure the *h*−*e* pair is stabilized into a charge-separated species as a result of the O−H and C−H cleavage reactions.

The adsorbed formaldehyde radical anion **1m** is the precursor of neutral adsorbed CH_2O, reported in some experiments.[16,76] However, the neutral adsorbed formaldehyde species is not stable in our stoichiometric model. This is due to the fact that the two O_{br} atoms carry the transferred hydrogen atoms, which implies that two electrons are injected in the 3d band of the TiO_2(110) surface. The CH_2O species acts as a sink for one of the electrons, reducing the *e*−*e* repulsion in the 3d band. This is in contrast to a formally stoichiometric TiO_2(110) surface without $O_{br}H$ groups, where it is possible to locate a neutral adsorbed formaldehyde species.[64] Therefore, to complete the formation of neutral formaldehyde from **1m** a further photochemical step may be necessary consisting of the excitation of the CH_2O excess electron, as found in some experiments.[16] Alternatively, the process may be completed thermally through CH_2O or H_2 desorption.[12,17] In any case, the transformation of adsorbed methanol to adsorbed formaldehyde radical anion (**1a**−**1m**) corresponds to transfer of two protons and one electron to the substrate induced by one photon.

4. CONCLUSIONS

Our study provides two main significant and novel insights into the photocatalytic oxidation of methanol on rutile TiO_2(110). First, we show the role of excitonic states in the initial PCET step and their importance for the efficiency. This goes beyond the generally accepted photocatalytic model which invokes charge carrier separation prior to the oxidation or reduction at the interface between the substrate and the adsorbate.[2] Second, we present a novel one-photon mechanism for the direct formation of formaldehyde from adsorbed methanol. Photoinduced excitonic interfacial PCET is synonymous with the formation of the excited-state adsorbed methoxy radical intermediate, which is directly connected to the adsorbed formaldehyde radical anion. This unambiguously identifies methanol as an active species in this process, as suggested by some experimental studies.[13,16] The lack of *h* trapping at adsorbed CH_3OH is often used to support the claim that methanol is not an active species for formaldehyde formation,[35] but our mechanism shows that CH_3OH is in fact an active species for formaldehyde formation.

Our results have revealed that excitons play a fundamental role in the photocatalytic oxidation of organic adsorbates on TiO_2, a process relevant in energy, environmental and synthetic technologies based on heterogeneous photocatalysis. Although the calculations consider CH_3OH adsorbed under UHV conditions, the excitonic mechanism may also explain the photooxidation of other organic protic adsorbates under UHV conditions or in solution. In future work we will also investigate its validity for the first step of photocatalytic water oxidation.

■ ASSOCIATED CONTENT

Supporting Information

The Supporting Information is available free of charge on the ACS Publications website at DOI: 10.1021/jacs.6b11067.

Ground-state O−H and C−H dissociation paths, interpolation between *h*-shared and *h*-localized minima of CH_3O@TiO_2(110), and evolution of O−Ti_{cus} distance along representative coordinates, larger images of the T_1 and S_0 spin densities shown in Figure 4 (PDF)

■ AUTHOR INFORMATION

Corresponding Authors

*annapaola.migani@icn2.cat
*lluis.blancafort@udg.edu

ORCID

Annapaola Migani: 0000-0001-5422-805X
Lluís Blancafort: 0000-0002-0003-5540

Notes

The authors declare no competing financial interest.

■ ACKNOWLEDGMENTS

We acknowledge financial support from Spanish Ministerio de Economía y Competitividad (FIS2012-37549-C05-02, UNGI10-4E-801, RYC-2011-09582, CTQ2015-69363-P), Generalitat de Catalunya (2014SGR-301, 2014SGR-1202, XRQTC), and computational time from BSC Red Española de Supercomputación and Consorci de Serveis Universitaris de Catalunya.

■ REFERENCES

(1) Fujishima, A.; Honda, K. *Nature* **1972**, *238*, 37−38.
(2) Henderson, M. A. *Surf. Sci. Rep.* **2011**, *66*, 185−297.
(3) Thompson, T. L.; John, T.; Yates, J. *Chem. Rev.* **2006**, *106*, 4428−4453.
(4) Friend, C. M. *Chemical record (New York, N.Y.)* **2014**, *14*, 944−951.
(5) Tan, S.; Feng, H.; Ji, Y.; Wang, Y.; Zhao, J.; Zhao, A.; Wang, B.; Luo, Y.; Yang, J.; Hou, J. G. *J. Am. Chem. Soc.* **2012**, *134*, 9978−9985.
(6) Yang, W.; Wei, D.; Jin, X.; Xu, C.; Geng, Z.; Guo, Q.; Ma, Z.; Dai, D.; Fan, H.; Yang, X. *J. Phys. Chem. Lett.* **2016**, *7*, 603−608.
(7) Zhou, C.; Ren, Z.; Tan, S.; Ma, Z.; Mao, X.; Dai, D.; Fan, H.; Yang, X.; LaRue, J.; Cooper, R.; et al. *Chem. Sci.* **2010**, *1*, 575−580.
(8) Guo, Q.; Xu, C.; Ren, Z.; Yang, W.; Ma, Z.; Dai, D.; Fan, H.; Minton, T. K.; Yang, X. *J. Am. Chem. Soc.* **2012**, *134*, 13366−13373.
(9) Zhou, C.; Ma, Z.; Ren, Z.; Wodtke, A. M.; Yang, X. *Energy Environ. Sci.* **2012**, *5*, 6833−6844.
(10) Xu, C.; Yang, W.; Ren, Z.; Dai, D.; Guo, Q.; Minton, T. K.; Yang, X. *J. Am. Chem. Soc.* **2013**, *135*, 19039−19045.
(11) Phillips, K. R.; Jensen, S. C.; Baron, M.; Li, S.-C.; Friend, C. M. *J. Am. Chem. Soc.* **2013**, *135*, 574−577.

DOI: 10.1021/jacs.6b11067
J. Am. Chem. Soc. 2016, 138, 16165−16173

(12) Xu, C.; Yang, W.; Guo, Q.; Dai, D.; Chen, M.; Yang, X. *J. Am. Chem. Soc.* **2013**, *135*, 10206−10209.
(13) Yuan, Q.; Wu, Z.; Jin, Y.; Xu, L.; Xiong, F.; Ma, Y.; Huang, W. *J. Am. Chem. Soc.* **2013**, *135*, 5212−5219.
(14) Guo, Q.; Xu, C.; Yang, W.; Ren, Z.; Ma, Z.; Dai, D.; Minton, T. K.; Yang, X. *J. Phys. Chem. C* **2013**, *117*, 5293−5300.
(15) Wang, Z.-q.; Hao, Q.-q.; Zhou, C.-y.; Dai, D.-x.; Yang, X.-m. *Chin. J. Chem. Phys.* **2015**, *28*, 459−464.
(16) Wei, D.; Jin, X.; Huang, C.; Dai, D.; Ma, Z.; Li, W.-X.; Yang, X. *J. Phys. Chem. C* **2015**, *119*, 17748−17754.
(17) Feng, H.; Tan, S.; Tang, H.; Zheng, Q.; Shi, Y.; Cui, X.; Shao, X.; Zhao, A.; Zhao, J.; Wang, B. *J. Phys. Chem. C* **2016**, *120*, 5503−5514.
(18) Kawai, T.; Sakata, T. *J. Chem. Soc., Chem. Commun.* **1980**, 694−695.
(19) Yang, X.; Zhang, A.; Gao, G.; Han, D.; Han, C.; Wang, J.; Lu, H.; Liu, J.; Tong, M. *Catal. Commun.* **2014**, *43*, 192−196.
(20) Xiong, F.; Yu, Y.-Y.; Wu, Z.; Sun, G.; Ding, L.; Jin, Y.; Gong, X.-Q.; Huang, W. *Angew. Chem.* **2016**, *128*, 633−638.
(21) Amtout, A.; Leonelli, R. *Phys. Rev. B: Condens. Matter Mater. Phys.* **1995**, *51*, 6842−6851.
(22) Pascual, J.; Camassel, J.; Mathieu, H. *Phys. Rev. B: Condens. Matter Mater. Phys.* **1978**, *18*, 5606−5614.
(23) Chen, C.; Shi, T.; Chang, W.; Zhao, J. *ChemCatChem* **2015**, *7*, 724−731.
(24) Schrauben, J. N.; Hayoun, R.; Valdez, C. N.; Braten, M.; Fridley, L.; Mayer, J. M. *Science* **2012**, *336*, 1298−1301.
(25) Chen, J.; Li, Y.-F.; Sit, P.; Selloni, A. *J. Am. Chem. Soc.* **2013**, *135*, 18774−18777.
(26) Petek, H.; Zhao, J. *Chem. Rev.* **2010**, *110*, 7082−7099.
(27) Venkataraman, C.; Soudackov, A. V.; Hammes-Schiffer, S. *J. Phys. Chem. C* **2010**, *114*, 487−496.
(28) Li, B.; Zhao, J.; Onda, K.; Jordan, K. D.; Yang, J.; Petek, H. *Science* **2006**, *311*, 1436−1440.
(29) Valentin, C. D.; Fittipaldi, D. *J. Phys. Chem. Lett.* **2013**, *4*, 1901−1906.
(30) Ji, Y.; Wang, B.; Luo, Y. *J. Phys. Chem. C* **2014**, *118*, 21457−21462.
(31) Valentin, C. D. *J. Phys.: Condens. Matter* **2016**, *28*, 074002.
(32) Ji, Y.; Wang, B.; Luo, Y. *J. Phys. Chem. C* **2012**, *116*, 7863−7866.
(33) Ji, Y.; Wang, B.; Luo, Y. *J. Phys. Chem. C* **2014**, *118*, 1027−1034.
(34) Chu, W.; Saidi, W. A.; Zheng, Q.; Xie, Y.; Lan, Z.; Prezhdo, O. V.; Petek, H.; Zhao, J. *J. Am. Chem. Soc.* **2016**, *138*, 13740−13749.
(35) Shen, M.; Henderson, M. A. *J. Phys. Chem. Lett.* **2011**, *2*, 2707−2710.
(36) Kolesov, G.; Vinichenko, D.; Tritsaris, G. A.; Friend, C. M.; Kaxiras, E. *J. Phys. Chem. Lett.* **2015**, *6*, 1624−1627.
(37) Krukau, A. V.; Vydrov, O. A.; Izmaylov, A. F.; Scuseria, G. E. *J. Chem. Phys.* **2006**, *125*, 224106.
(38) Heyd, J.; Scuseria, G. E.; Ernzerhof, M. *J. Chem. Phys.* **2003**, *118*, 8207.
(39) Wang, L.-Q.; Ferris, K. F.; Winokur, J. P.; Shultz, A. N.; Baer, D. R.; Engelhard, M. H. *J. Vac. Sci. Technol., A* **1998**, *16*, 3034−3040.
(40) Migani, A.; Mowbray, D. J.; Iacomino, A.; Zhao, J.; Petek, H.; Rubio, A. *J. Am. Chem. Soc.* **2013**, *135*, 11429−11432.
(41) Migani, A.; Mowbray, D. J.; Zhao, J.; Petek, H.; Rubio, A. *J. Chem. Theory Comput.* **2014**, *10*, 2103−2114.
(42) Migani, A.; Mowbray, D. J. *Comput. Theor. Chem.* **2014**, *1040*−*1041*, 259−265.
(43) Sun, H.; Mowbray, D. J.; Migani, A.; Zhao, J.; Petek, H.; Rubio, A. *ACS Catal.* **2015**, *5*, 4242−4254.
(44) Kresse, G.; Joubert, D. *Phys. Rev. B: Condens. Matter Mater. Phys.* **1999**, *59*, 1758.
(45) Migani, A.; Mowbray, D. J.; Zhao, J.; Petek, H. *J. Chem. Theory Comput.* **2015**, *11*, 239−251.
(46) Mowbray, D. J.; Migani, A. *J. Phys. Chem. C* **2015**, *119*, 19634−19641.
(47) Mowbray, D. J.; Migani, A. *J. Phys. Chem. C* **2016**, *120*, 4151−4151.
(48) Mowbray, D. J.; Migani, A. *J. Chem. Theory Comput.* **2016**, *12*, 2843−2852.
(49) Salpeter, E. E.; Bethe, H. A. *Phys. Rev.* **1951**, *84*, 1232−1242.
(50) van Setten, M. J.; Gremaud, R.; Brocks, G.; Dam, B.; Kresse, G.; de Wijs, G. A. *Phys. Rev. B: Condens. Matter Mater. Phys.* **2011**, *83*, 035422.
(51) Burdett, J. K.; Hughbanks, T.; Miller, G. J.; Richardson, J. W.; Smith, J. V. *J. Am. Chem. Soc.* **1987**, *109*, 3639−3646.
(52) Sheppard, D.; Xiao, P.; Chemelewski, W.; Johnson, D. D.; Henkelman, G. *J. Chem. Phys.* **2012**, *136*, 074103.
(53) Curtarolo, S.; Setyawan, W.; Hart, G. L.; Jahnatek, M.; Chepulskii, R. V.; Taylor, R. H.; Wang, S.; Xue, J.; Yang, K.; Levy, O.; et al. *Comput. Mater. Sci.* **2012**, *58*, 218−226.
(54) Carchini, G.; Lopez, N. *Phys. Chem. Chem. Phys.* **2014**, *16*, 14750−14760.
(55) de Armas, R. S.; Oviedo, J.; San Miguel, M. A.; Sanz, J. F. *J. Phys. Chem. C* **2007**, *111*, 10023−10028.
(56) Hammes-Schiffer, S.; Stuchebrukhov, A. A. *Chem. Rev.* **2010**, *110*, 6939−6960.
(57) Migani, A.; Bearpark, M. J.; Olivucci, M.; Robb, M. A. *J. Am. Chem. Soc.* **2007**, *129*, 3703−3713.
(58) Migani, A.; Blancafort, L.; Robb, M. A.; DeBellis, A. D. *J. Am. Chem. Soc.* **2008**, *130*, 6932−6933.
(59) Migani, A.; Leyva, V.; Feixas, F.; Schmierer, T.; Gilch, P.; Corral, I.; Gonzalez, L.; Blancafort, L. *Chem. Commun.* **2011**, *47*, 6383−6385.
(60) Li, Q.; Migani, A.; Blancafort, L. *Phys. Chem. Chem. Phys.* **2012**, *14*, 6561−6568.
(61) Sinicropi, A.; Migani, A.; De Vico, L.; Olivucci, M. *Photochem. Photobiol. Sci.* **2003**, *2*, 1250−1255.
(62) Liu, S.; Liu, A.-a.; Wen, B.; Zhang, R.; Zhou, C.; Liu, L.-M.; Ren, Z. *J. Phys. Chem. Lett.* **2015**, *6*, 3327−3334.
(63) Cheng, J.; VandeVondele, J.; Sprik, M. *J. Phys. Chem. C* **2014**, *118*, 5437−5444.
(64) Liu, L.; Zhao, J. *Surf. Sci.* **2016**, *652*, 156−162.
(65) Fujishima, A.; Zhang, X.; Tryk, D. A. *Surf. Sci. Rep.* **2008**, *63*, 515−582.
(66) Salvador, P. *J. Phys. Chem. C* **2007**, *111*, 17038−17043.
(67) Tamaki, Y.; Furube, A.; Murai, M.; Hara, K.; Katoh, R.; Tachiya, M. *J. Am. Chem. Soc.* **2006**, *128*, 416−417.
(68) Bernardi, F.; Olivucci, M.; Robb, M. A. *Chem. Soc. Rev.* **1996**, *25*, 321−328.
(69) Migani, A.; Olivucci, M. In *Conical Intersections: Electronic Structure, Dynamics & Spectroscopy*; Domcke, W., Yarkony, D. R., Köppel, H., Eds.; Advanced Series in Physical Chemistry 15; World Scientific: Singapore, 2004; Vol. *15*; pp 271−320.
(70) Li, Q.; Migani, A.; Blancafort, L. *J. Phys. Chem. Lett.* **2012**, *3*, 1056−1061.
(71) Migani, A.; Robb, M. A.; Olivucci, M. *J. Am. Chem. Soc.* **2003**, *125*, 2804−2808.
(72) Weingart, O.; Migani, A.; Olivucci, M.; Robb, M. A.; Buss, V.; Hunt, P. *J. Phys. Chem. A* **2004**, *108*, 4685−4693.
(73) Li, Q.; Mendive-Tapia, D.; Paterson, M. J.; Migani, A.; Bearpark, M. J.; Robb, M. A.; Blancafort, L. *Chem. Phys.* **2010**, *377*, 60−65.
(74) Blancafort, L. *ChemPhysChem* **2014**, *15*, 3166−3181.
(75) Goodrow, A.; Bell, A. T.; Head-Gordon, M. *J. Phys. Chem. C* **2009**, *113*, 19361−19364.
(76) Yuan, Q.; Wu, Z.; Jin, Y.; Xiong, F.; Huang, W. *J. Phys. Chem. C* **2014**, *118*, 20420−20428.

DOI: 10.1021/jacs.6b11067
J. Am. Chem. Soc. 2016, 138, 16165−16173